Journal of Fluids and Structures 17 (2003) 955–970

JOURNAL OF FLUIDS AND STRUCTURES

www.elsevier.nl/locate/jnlabr/yjfls

Self-excited oscillations of turbulent inflow along a perforated plate

C. Ozalp[a,1], A. Pinarbasi[a,2], D. Rockwell[b,*]

[a] *Cukurova University, Adana, Turkey*

[b] *Department of Mechanical Engineering and Mechanics, Lehigh University, 354 Packard Laboratory 19 Memorial Drive, Bethlehem, PA 18015 3085, USA*

Received 1 October 2002; accepted 7 March 2003

Abstract

The grazing flow of a fully turbulent boundary layer along a perforated plate, which is bounded by a closed cavity on its backside, can give rise to highly coherent, self-sustained oscillations of the shear flow, even in absence of acoustic resonant or fluid elastic effects. These oscillations are characterized in terms of unsteady pressure fluctuations and quantitative images of the instantaneous and averaged flow structure using a technique of high-image-density particle image velocimetry. This purely hydrodynamic instability, which rapidly emerges above the turbulent background, has a wavelength that is much longer than the hole diameter of the perforated plate. Variations of the effective length L of the perforated plate show nearly invariant values of dimensionless frequency fL/U, in which f is the predominant frequency of oscillation and U is the freestream velocity. In fact, this relationship holds even when the diameter of the hole pattern is altered. Variation of the hole diameter D does, however, strongly influence the amplitude and degree of organization of the self-sustained oscillation. It is demonstrated that, as the hole diameter becomes larger relative to the inflow boundary layer thickness, the amplitude of the predominant spectral peak is substantially attenuated and, in a limiting case, undetectable. These features are interpreted in conjunction with instantaneous and averaged patterns of the flow structure, which include distributions of both Reynolds stress and amplitudes of spectral peaks.

This type of instability is distinctively different from the classical instability associated with "singing" of perforated plates employed in attenuation liners in engineering systems, where the genesis of the instability is local vortex shedding within each hole of the perforation, in contrast to the long wavelength instability that is addressed herein.

1. Introduction

1.1. Previous related investigations

Perforated surfaces, plates, and interfaces are often employed for attenuation of sound in internal flow systems. Such perforated surfaces are commonly found in the exhaust system of an automobile, within aircraft engines and compressors, as well as in reciprocating engine systems and ventilation units. Such perforated surfaces can be effective for attenuation of narrow-band noise or sound. Depending upon the parameters of the perforated surface and the inflow, adverse effects can occur, including the onset of "singing", or pure tone noise generation. Meyer et al. (1958)

*Corresponding author. Tel.: +1-610-758-4107; fax: +1-610-758-4041.
E-mail address: dor0@lehigh.edu (D. Rockwell).

[1] On leave as Visiting Research Scientist at Lehigh University.

[2] On leave as Fulbright Research Scholar at Lehigh University.

0889-9746/03/$ - see front matter
doi:10.1016/S0889-9746(03)00045-8

found that self-excited generation of tones could occur over two ranges of flow velocity, one corresponding to resonance coupled with the Helmholtz resonator on the opposite side of the perforated plate, and another coupled with a resonant mode of the main flow duct. Dean (1972) and Adams (1974) also observed self-excited pure tone generation due to flow past perforated liners. The possible importance of the scale and spacing of the individual perforations was pointed out by Dean (1972). Tsui and Flandro (1977) report the occurrence of "singing", which they attribute to vortex shedding past the holes; they found that this phenomenon could be due to coupling with either a resonant mode of the cavity on the backside of the plate or an acoustic mode(s) of the main flow duct. Bauer and Chapkis (1977) also investigated various features of pure tone noise generation due to flow past perforated surfaces. The importance of the instability past an individual hole, or orifice, which can involve vortex shedding, was pursued by Ronneberger (1980). In his investigation, he applied an external perturbation to a single rectangular cavity, in order to induce an oscillation of the interface along the cavity, with the intent of simulating the self-excited vortex shedding that occurs during coupled resonance in an actual orifice of a perforated plate.

From a design standpoint, it is important to know the impedance of a perforated plate that is subjected to tangential inflow. Dickey et al. (2001) employed a loudspeaker to induce pure tone, external excitation of a side branch, with a perforated plate mounted along its open end. The grazing flow was represented in terms of the friction velocity, and the distinctive features of a circular orifice, relative to a louver, were characterized. Grazing flow past perforated plates can also generate substantial broadband noise, even when pure tone generation is not an issue. Nelson (1982) employed experimental data in conjunction with a model to predict the broadband noise level.

If the perforated plate undergoes vibrations, then a number of interesting issues arise. As found by Howe (1996), vorticity generation in the apertures of a perforated plate subjected to a grazing flow can lead to dissipation of plate vibrations. In a further theoretical study, Howe (1997) determined the sound production arising from both turbulence and vortex shedding. Maung et al. (1999) performed experiments on a vibrating perforated plate in a flow at high Reynolds number, and characterized the damping characteristics.

The importance of perforated plates is not limited to low speed applications. Occurrence of high noise levels in transonic wind tunnels is well known, and recent results related to suppression of edge-tone type noise in the systems is described by Medved (1993).

A further, related configuration, which can be associated with pure tone generation, involves either one or three spanwise (two-dimensional) obstacles across the opening of a resonant cavity, as addressed by Zoccola (2002). An acoustic resonant mode of the cavity was excited by, and coupled with, the flow instability(ies) along the obstacle(s).

In nearly all of the foregoing investigations, emphasis has been on the genesis of either pure tone or broadband noise in relation to localized interaction of the separated shear flow past individual holes, orifices, or gaps. In the case of pure tone generation, the inherent instability of the separated shear layer past, for example, the hole should scale on a characteristic length of the inflow boundary layer and is directly influenced by the diameter, or streamwise, length of the hole.

Recently, Celik and Rockwell (2003) have shown that a long wavelength, self-excited instability can arise due to essentially laminar inflow past a perforated plate. In essence, they found that the wavelength of the instability is much larger than the diameter of the individual holes in a perforated plate of relatively large open area ratio. This instability occurred in the presence of a large, single cavity on the backside of the perforated plate, and the system parameters were such that neither acoustic resonance nor wall elasticity effects were present; that is, the self-excited oscillation was due to purely hydrodynamic effects. This preliminary investigation was limited to oscillations arising in a laminar inflow; in contrast, the present investigation addresses self-excited oscillations arising within a fully developed turbulent inflow. Furthermore, the investigation of Celik and Rockwell (2003) focused on a single hole diameter of the perforated plate, and addressed only instantaneous representations of the flow patterns, along with determination of the predominant frequency of oscillation as a function of effective length of the perforated plate. The present investigation addresses variations of hole diameter in the context of time-averaged statistics of the flow unsteadiness.

1.2. Unresolved issues

An issue of central importance is whether highly coherent, self-sustained oscillations, which have a relatively long wavelength, can occur due to a fully turbulent inflow past a perforated plate. If the inherent instability mechanism of the shear flow past the perforations of the plate is sufficiently robust, then one expects it to rapidly emerge above the background turbulence of the inflow boundary layer. In addition, the effect of the diameter of the individual holes in the perforated plate has not been addressed. If the open area ratio of the perforated plate is held constant, while the hole diameter is varied, it should be possible to determine the effect of diameter on the degree of organization of the self-excited oscillations.

If a self-excited instability does arise, even in presence of turbulent inflow, the issue arises as to whether the frequency can be scaled according to an effective length of the perforated plate, irrespective of the hole diameter. If so, this would reinforce the view of the instability as a long wavelength phenomenon.

Characterization of the instability in terms of patterns of instantaneous and averaged Reynolds stress has not been pursued. Furthermore, the spectral content of the fluctuating velocities across the shear flow has not yet been addressed. This type of assessment, in conjunction with a cross-spectral analysis to yield phase information, could provide insight into the wave-like character of the fluctuation across the nominally turbulent shear flow.

Instantaneous and averaged statistical representations of the unsteady flow pattern in the vicinity of the trailing-end (edge) of the perforated plate are particularly important. If indeed long wavelength instability does occur along the perforated plate, and if it scales on the plate length, the existence of a feedback mechanism would be suggested; it must have its origin in an unsteady flow mechanism at the end of the plate.

The overall aim of this investigation is to address the unresolved issues described in the foregoing, by use of a technique of high-image-density particle image velocimetry, in conjunction with pressure measurements at the trailing-end of the perforated plate.

2. Experimental system and techniques

Experiments were undertaken in a large-scale water channel, which had a test-section 4928 mm long, 610 mm deep and 927 mm wide. This main test-section of the channel was preceded by a large reservoir, then a flow-conditioning unit that involved a sequence of honeycomb and screens, and finally a contraction.

A test-section insert, which was placed within the main test-section of the water channel, involved an additional contraction, which brought the width of the channel from its original value of 927 mm to an effective channel width of 387 mm. A long flat plate was located downstream of this contraction. The length of this plate, which extended from the exit of the contraction to the leading-edge of the perforated plate of interest in the present investigation, was 1575 mm. In order to rapidly trip the boundary layer, a sequence of eleven boundary layer trips were placed at and near the leading-edge of the plate. These trips were based on the design criteria of the Johansen and Smith (1983). Small spherical and circular cylindrical elements made up successive arrays, which allowed generation of a fully developed turbulent boundary layer at the leading-edge of the perforated plate investigated herein. The freestream velocity was maintained at a value $U = 240$ mm/s and the momentum thickness of the turbulent boundary layer was $\theta = 75$ mm. The Reynolds number based on θ was $\mathrm{Re}_\theta = 1800$. The form of this inflow boundary layer agreed very well with that defined by Lin and Rockwell (2001) in a related investigation involving fully developed turbulent flow.

The perforated plate was mounted in a vertical plate of height $H_p = 457.2$ mm, as defined in the schematic of Fig. 1. The free-surface of the water in the test-section was 180 mm above the top edge of the plate. The spanwise length l_a and the streamwise length l_b of the plate had nominal values of 197 and 183 mm, respectively. The thickness t of the perforated plate was 11 mm. In order to vary the effective length L of the plate, a large-scale impingement plate could be translated along its surface, as illustrated in Fig. 1. This impingement plate had a sharp edge beveled at an angle of 10°.

The perforated plate system of Fig. 1 was bounded on its backside by a large-scale cavity, which is defined in the schematic by a rectangular pattern of dashed lines. This cavity was sealed to the vertical plate that contained the perforated plate. The size of this cavity was substantially larger than the width and length of the perforated plate, such that the consequence of localized recirculation flow patterns was minimal. The length of the cavity in the streamwise direction was 610 mm, its height was 432 mm and its depth was 432 mm. Since purely hydrodynamic oscillations are of interest, the cavity was designed with rigid walls, in order to preclude fluid elastic effects. In addition, the characteristic frequencies generated in this study have values of acoustic wavelength roughly two orders of magnitude larger than the largest dimension of the cavity; on this basis, the effects of resonant acoustic coupling were eliminated.

A close-up of the perforation pattern in the plate is given in Fig. 2. This overview also defines the effective streamwise length L of the plate and the location of the unsteady pressure measurement referred to in Fig. 1. The diameter of each hole is designated as D, which had values of $D = 6.4$, 12.7, 19.1 and 25.4 mm. The spanwise and longitudinal spacings Δ_a and Δ_b had values such that the open area ratio of all hole patterns was the same. This open area ratio was 69%; it is defined as the total open area due to the sum of the areas of the holes, normalized by the total area of the plate.

Unsteady pressure measurements at the tip of the impingement plate involved placement of a high sensitivity pressure transducer within a brass tube arrangement along the top edge of the perforated plate. Initial calibrations showed that the effective amplitude and phase distortion of the measured pressure was less than 1% of their nominal values. Pressure signals were acquired using a PCB transducer, model number 106B50. Spectra of the fluctuating pressure were acquired through sampling the pressure signal at a nominal frequency of $\Delta f = 20$ Hz, which provides a Nyquist frequency $1/2\ \Delta f = 10$ Hz.

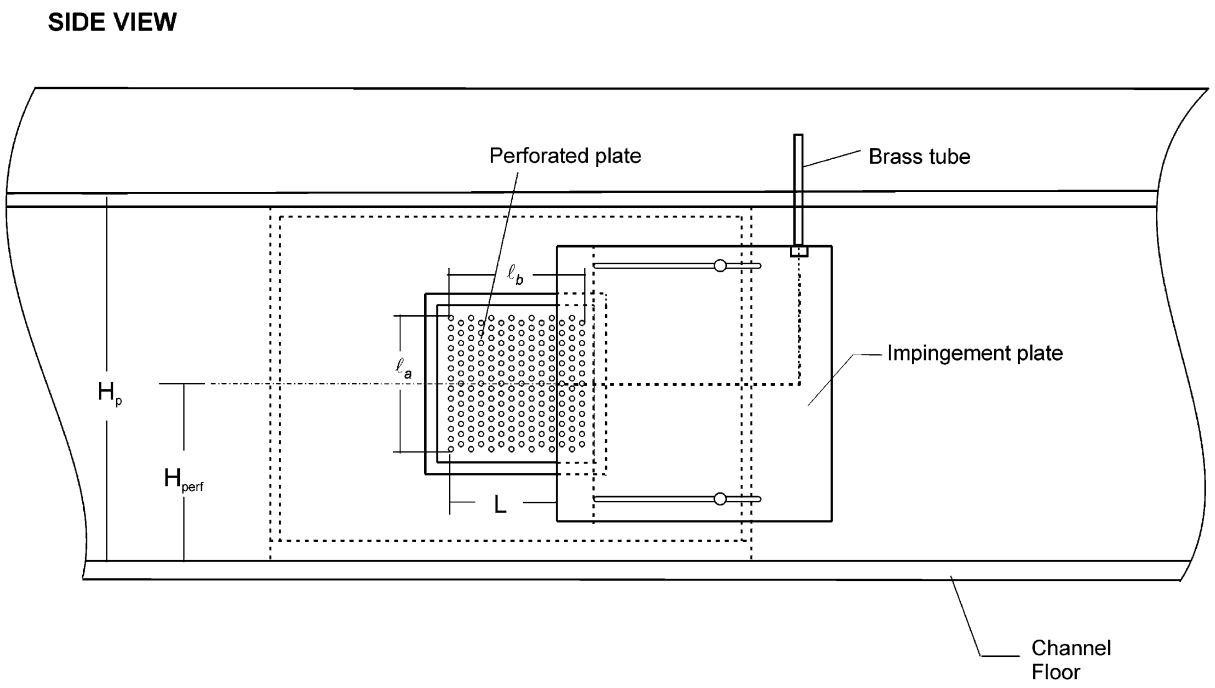

Fig. 1. View of perforated plate and impingement plate.

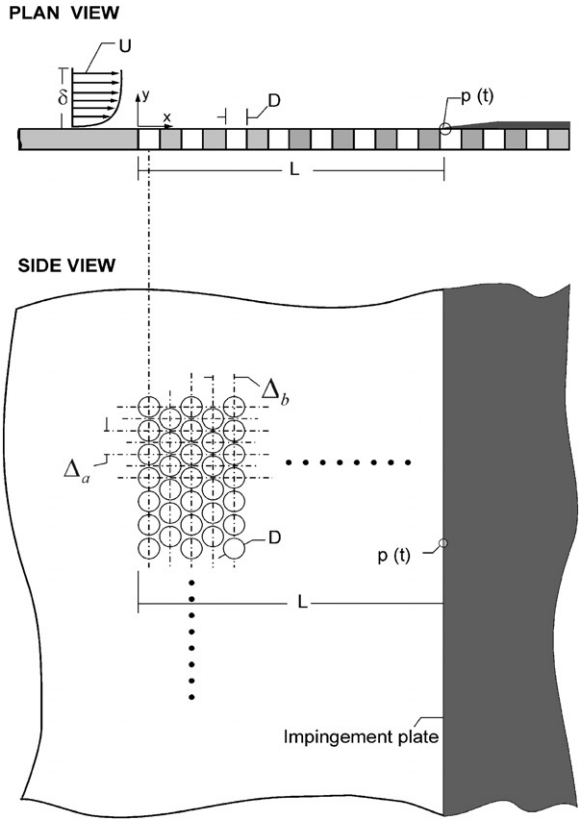

Fig. 2. Schematic of perforated plate showing pattern and scales of holes.

Quantitative visualization of the flow patterns was attained using a method of high-image-density particle image velocimetry. Illumination was in the form of a 1 mm thick laser sheet which was generated from two Nd:Yag pulsed lasers fitted with a cylindrical–spherical lens system. Each laser of the dual system had a power rating of 90 mJ. Two orientations of this sheet were employed. For the horizontal orientation, the laser sheet intersected the horizontal center-line of the plate, as indicated in Fig. 3. This placement of the laser allowed quasi-two-dimensional visualization of the flow structure. Alternately, a horizontal orientation of the laser sheet was used, as indicated in Fig. 10. In this case, the sheet was placed close to the surface of the perforated plate, i.e., the distance between the center-line of the laser sheet and the surface of the plate was 1 mm. Using this approach, it is possible to determine the instantaneous spanwise structure of the flow pattern along the perforated plate.

The flow was seeded with 12 μm, metallic coated hollow plastic spheres, which were essentially neutrally buoyant. A digital camera, having a resolution of 1024×1024 pixels, allowed acquisition of the patterns of particle images. The pattern of velocity vectors was calculated by performing a cross-correlation of the particle images in each frame pair. During this interrogation, windows of 32×32 pixels and 16×16 pixels were employed. In order to ensure that the criterion for high-image-density was satisfied, the number of particle images within the interrogation window was, at minimum, 15–20. Furthermore, during the interrogation process, these windows were overlapped by 50% in order to satisfy the Nyquist criterion. The field of view for the velocity vectors is indicated in the schematic of each figure. The total number of velocity vectors acquired over the field of view of each original image ranged from 9136 to 9364. Herein, emphasis is on the vorticity-bearing layer of the flow immediately adjacent to the perforated plate, and only this portion of the original field of view is shown. Regarding uncertainty of the values of velocity and vorticity obtained using the PIV method, the uncertainty on velocity is estimated to be within 1% and vorticity to be within 5%.

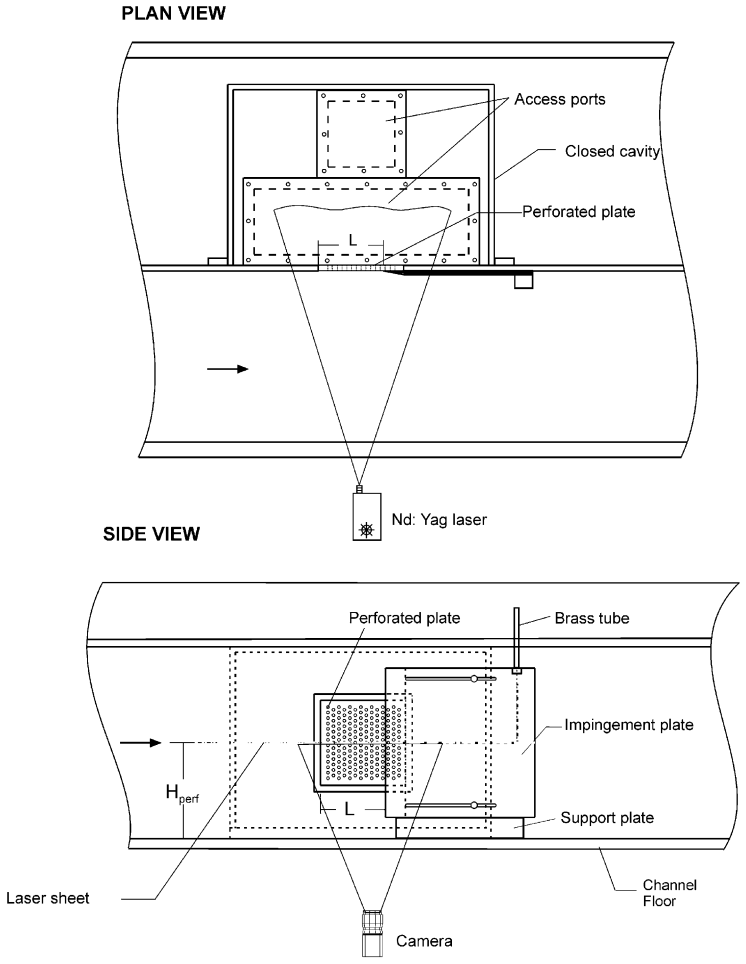

Fig. 3. Plan and side views of test-section showing location and orientation of laser sheet and field of view of camera.

The PIV images were recorded in the cinema mode, at an effective framing rate of 15 frames per second. Since the maximum frequency of interest in this investigation corresponded to a coherent oscillation at $f_o \leqslant 1$ Hz, it was possible to perform spectral analysis. At a specified location, xy in the flow field, it was possible to construct the time variation of the desired velocity fluctuation by considering a total of 200 PIV images, which represents 200 sample points. This single record, without averaging, was employed to determine the spectrum. A Hanning window was employed during the spectral analysis.

3. Averaged Reynolds stress of shear flow past a perforated plate

Fig. 4 compares patterns of time-averaged Reynolds stress $\langle u'v' \rangle / U^2$ for two extreme values of hole size of the perforated plate: $D/\theta = 0.85$ and 3.38. The field of view of these patterns is indicated by the dashed frame in the schematic. The coordinate system (x', y') is measured from the leading-corner of this field of view, while the system (x, y) is from the leading-edge of the perforated plate. For the case of the smallest hole $D/\theta = 0.85$, represented by the top set of contours, high levels occur in the region close to the plate perforation. In fact, the extrema of $\langle u'v' \rangle / U^2$ occur within a layer approximately 0.5θ from the surface of the perforated plate. Furthermore, the contours of $\langle u'v' \rangle / U^2$ near the impingement edge are spatially periodic in the region adjacent to the plate. Their streamwise wavelength is of the order of the hole diameter.

On the other hand, for the pattern with relatively large diameter holes $D/\theta = 3.38$, shown in the bottom set of contours, highly concentrated contours, with relatively high peak values, do not occur in the region immediately adjacent to the surface of the plate. Rather, in the region immediately upstream of the plate extending from $x'/\theta = 5.0$ to 10.5, the contours are displaced significantly away from the surface of the plate. The peak value $\langle u'v' \rangle_{\max} / U^2$ is -2.0×10^{-3}, compared to the substantially higher value of -5.6×10^{-3} for the aforementioned case of the small-diameter hole pattern shown in the top image.

A common feature of both patterns of Reynolds stress shown in the two images of Fig. 4 is that the concentrated layer of $\langle u'v' \rangle / U^2$ is confined to a region approximately $y'/\theta = 1.5$. These highly concentrated layers are in contrast to the rather broadly distributed, but well-defined regions of $\langle u'v' \rangle / U^2$, extending approximately over the range y'/θ from 2 to 5. This region corresponds to the highest amplitudes of the broadband Reynolds stress in the naturally occurring turbulent boundary layer. In fact, the elevation of this layer and its peak values of $\langle u'v' \rangle / U^2$ are in general accord with those of a fully developed turbulent boundary layer generated in a similar type of test-section by Lin & Rockwell (2001).

The relatively large amplitude and the highly ordered form of the pattern of Reynolds stress contours, which occur immediately adjacent to the perforated plate for the smaller hole pattern (see top image of Fig. 4), suggest occurrence of an organized oscillation when the diameter of the hole is sufficiently small. In the next section, the degree of organization of the oscillation is addressed for this hole diameter, as well as for larger hole diameters. Spectral analyses of velocity and pressure signals serve as a basis for comparison.

4. Spectra of velocity and pressure: effect of hole diameter

Fig. 5 shows spectra of pressure fluctuations $S_p(f)$, measured at the tip of the impingement edge, for various hole diameters. These pressure spectra are compared with spectra $S_u(f)$ of the longitudinal velocity fluctuation component $\tilde{u}(t)$ measured across the shear layer, at a streamwise location $x = 0.8L$.

Consider, first of all, the peak amplitude of the pressure spectra for increasing values of hole diameter D/θ, as represented in the bottom row of plots of Fig. 5. As D/θ increases from 0.85 to 2.54, the peak amplitude decreases substantially and, at the largest hole diameter $D/\theta = 3.38$, an organized component is no longer detectable.

This same trend is, in fact, evident in the peak amplitudes of the velocity spectra S_u shown in the top of Fig. 5. Consider, for example, the bottom row of spectra S_u, corresponding to an elevation $y/\theta = 0.22$ above the surface of the perforated plate. For increasing values of hole diameter $D/\theta = 0.85$ to 2.54, the amplitude decreases substantially, as observed for the aforementioned pressure spectra. At the largest hole diameter $D/\theta = 3.38$, a distinct peak is no longer detectable. Furthermore, for a given value of D/θ, the peak amplitude of the organized component, which is indicated by the vertical dashed-line in each spectrum, and connected from one spectrum to the next by an inclined dashed-line, shows a decrease with increasing elevation y/θ from the surface of the perforated plate. It is, therefore, apparent that for the cases where a highly organized oscillation component does occur in the turbulent shear layer past the perforated plate, it persists for a value of the order of 1 momentum thickness θ, i.e., $y'/\theta \cong 1$, though it decreases in amplitude. This

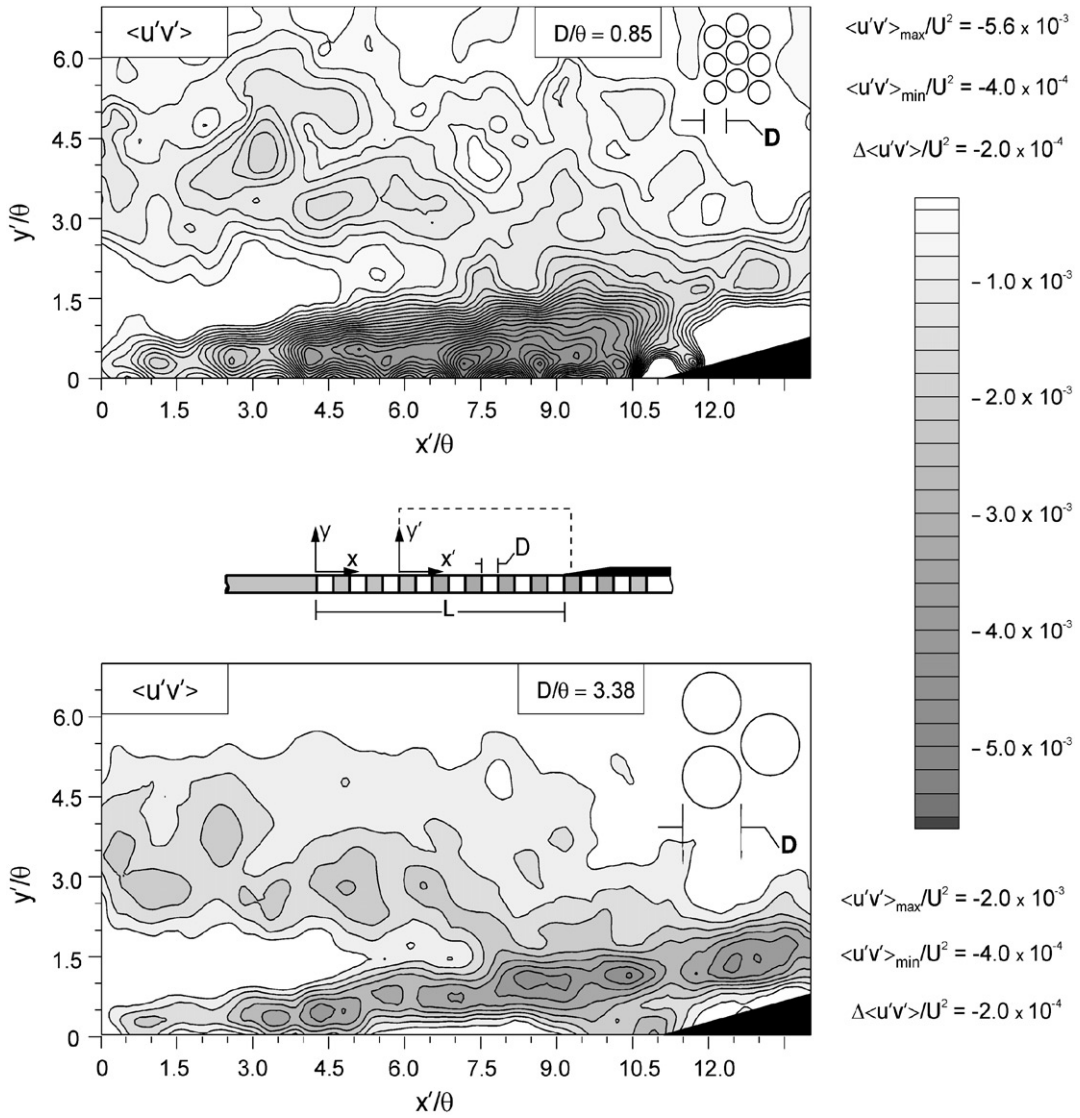

Fig. 4. Patterns of averaged Reynolds stress correlation $\langle u'v' \rangle / U^2$ for a relatively small diameter hole, $D/\theta = 0.85$ ($D = 6.4$ mm) and a relatively large diameter hole $D/\theta = 3.38$ ($D = 25.4$ mm). Minimum and incremental values are $[\langle u'v' \rangle / U^2]_{\min} = -4.0 \times 10^{-4}$ and $\Delta[\langle u'v' \rangle / U^2] = -2.0 \times 10^{-4}$. Peak values are $[\langle u'v' \rangle / U^2]_{\max} = -5.6 \times 10^{-3}$ for the small hole pattern, $D/\theta = 0.85$ and -2.0×10^{-3} for large hole pattern $D/\theta = 3.38$. Location of x' is at $x = 0.35L$. Length of perforated plate is $L/\theta = 17.2$.

observation is consistent with the highly concentrated layer of Reynolds stress $\langle u'v' \rangle / U^2$ shown for the smallest hole pattern at the top of Fig. 4.

Contours of constant amplitude of the spectral peak $|S_u(f_o)|$ of the longitudinal velocity fluctuation $\tilde{u}$, as well as the spectral peak $|S_v(f_o)|$ of the transverse $\tilde{v}$ fluctuation are given in Fig. 6. These patterns correspond to the smallest diameter hole $D/\theta = 0.85$. The streamwise location of these patterns corresponds to the region immediately upstream of, and including, the impingement edge. The amplitude of the spectral peak $|S_u(f_o)|$ attains peak values in the region immediately adjacent to the surface of the perforated plate, but contours of relatively high level extend well above the surface of the plate, at a streamwise location immediately upstream of the tip of the impingement edge.

Corresponding patterns of the distribution of the peak amplitude of the spectral component $|S_v(f_o)|$ are shown at the bottom of Fig. 6. This contour distribution of $|S_v(f_o)|$ is a complement to the pattern for the longitudinal component shown at the top of Fig. 6. It shows a highly ordered form, and the region very near the surface of the plate involves a

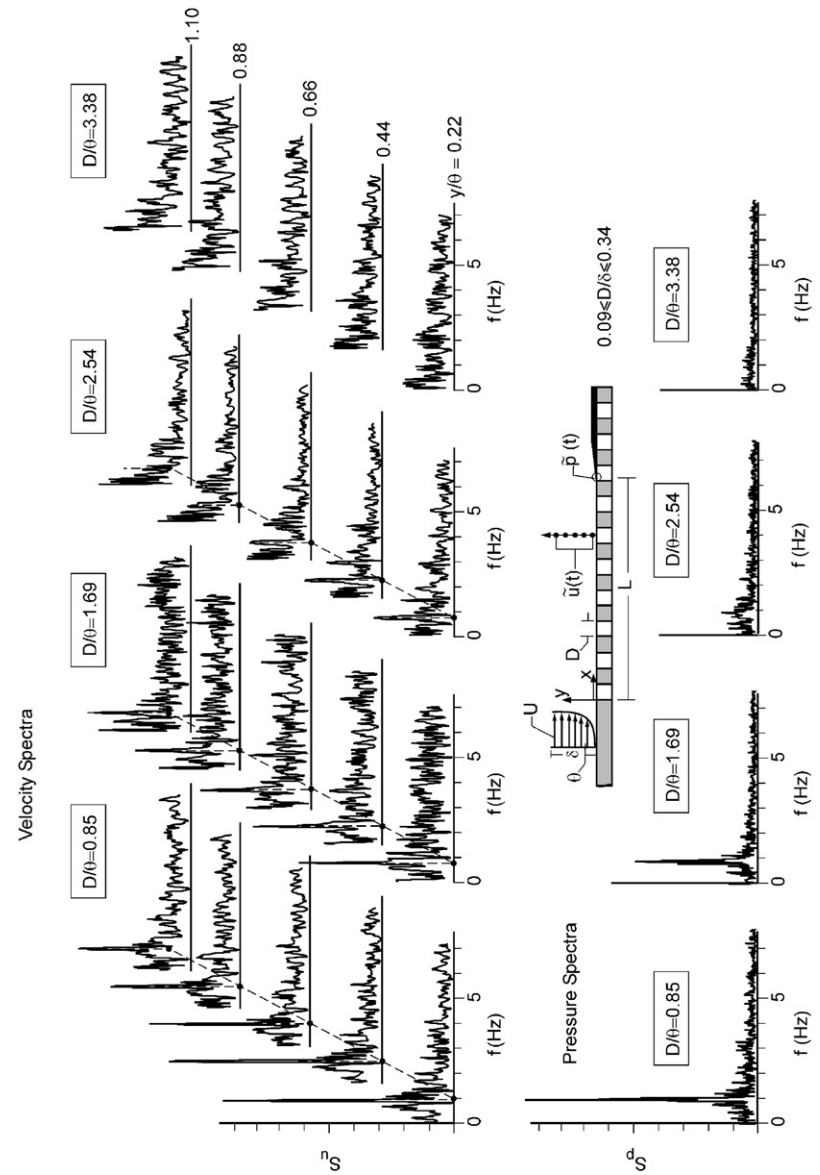

Fig. 5. Spectra of pressure fluctuation S_p at tip of impingement edge in relation to spectra of S_u of longitudinal velocity fluctuation across shear layer at a location $x = 0.8L$. Sets of spectra are shown for four different values of dimensionless diameter D/θ of the hole of the perforated plate. Length of plate is $L/\theta = 17.2$.

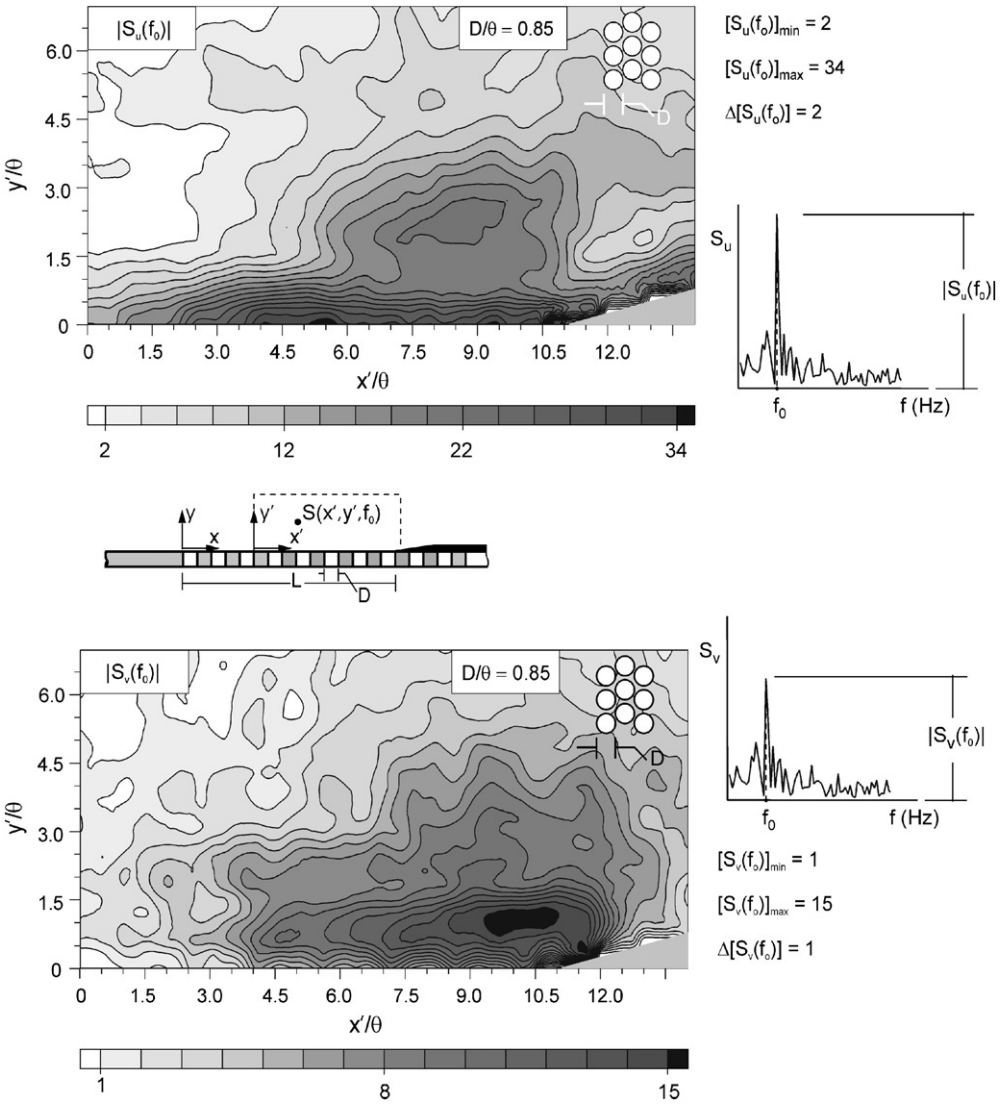

Fig. 6. Contours of constant amplitude of the dominant spectral peak $|S_u(f_o)|$ and $|S_v(f_o)|$ for the smallest diameter hole $D/\theta = 0.85$ of the perforated plate. $x' = 0$ at $x/L = 0.35$.

spatially periodic pattern with a wavelength approximately equal to the hole diameter. The highest amplitudes of $|S_v(f_o)|$ occur immediately adjacent to the tip of the impingement edge.

Taken together, the patterns of $|S_u(f_o)|$ and $|S_v(f_o)|$, shown at the top and bottom of Fig. 6, both exhibit peak values in the vicinity of the impingement edge. This observation suggests that the abrupt encounter of the incident organized wave with the tip of the impingement edge, which corresponds to the effective trailing-end of the perforated plate, generates an unsteady, highly organized flow distortion, which could act as an upstream influence that reinforces the self-sustained oscillation of the turbulent shear layer.

5. Scaling of organized component of oscillation

Spectra of the type shown in Fig. 5 were acquired for variations of the effective length of the perforated plate, expressed in normalized form as L/θ and L/D. This variation of L was accomplished by translating the tip of the

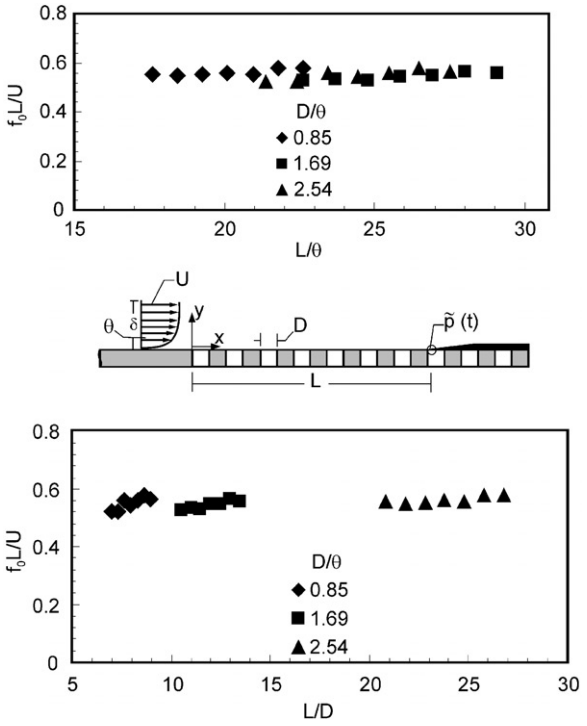

Fig. 7. Variation of dimensionless frequency f_o of dominant spectral peak of pressure fluctuation, normalized by effective length L of perforated plate and freestream velocity U, with respect to dimensionless cavity length L/θ and L/D, in which θ is momentum thickness of the approach flow and D is the diameter of the hole of the perforated plate. Dimensionless frequencies are shown for various D/θ values.

impingement edge along the surface of the perforated plate, as indicated in the schematic of Fig. 7. As a consequence, it is possible to determine the effect of variation of L/θ (or L/D) for various values of hole diameter D/θ. As shown in both of the plots of Fig. 7, the dimensionless frequency f_oL/U has a band of remarkably constant values lying within the range $f_oL/U = 0.50-0.60$. In other words, the dimensionless frequency f_oL/U is relatively insensitive to both L/θ (or L/D) and D/θ. This reaffirms the viewpoint that the instability along the surface of the perforated plate is a long wavelength phenomenon, and the effect of hole diameter D/θ is to alter the amplitude of the oscillation (see Fig. 5), but not its dimensionless frequency f_oL/U.

6. Form of organized wave along perforated plate

It is evident from the preceding section that a highly organized instability can exist in the nominally turbulent shear flow along the perforated plate. In order to determine the amplitude and phase distributions of this organized component across the shear layer, cross-spectral analysis was performed for the fluctuations of the longitudinal component $\tilde{u}(x_o, y, t)$, the transverse (vertical) component $\tilde{v}(x_o, y, t)$, and the vorticity $\tilde{w}(x_o, y, t)$. The amplitude distributions of each of these components are shown in Fig. 8a as a function of vertical distance y/θ from the surface of the plate, in comparison with the time-averaged longitudinal velocity $\bar{u}/U$. The corresponding phase angle variations are given in Fig. 8b. Whereas the phase $\phi_{\tilde{v}}$ of the transverse (vertical) component $\tilde{v}(x_o, y, t)$ exhibits only mild phase variations, the longitudinal phase $\phi_{\tilde{u}}$ shows a phase jump, i.e., a change in sign. The phase of the vorticity fluctuation $\phi_{\tilde{\omega}}$ increases substantially with distance from the surface of the perforated plate.

With the foregoing amplitude and phase distributions, it is possible to reconstruct the time-dependent variation of the longitudinal component of the wave-like motion. Distributions of instantaneous longitudinal velocity $\tilde{u}(x_o, y, t)$ are shown for sequential instants t/T during the oscillation cycle in the plot at the bottom left of Fig. 8c. These distributions were obtained from the distributions of amplitude and phase given in Figs. 8a and b.

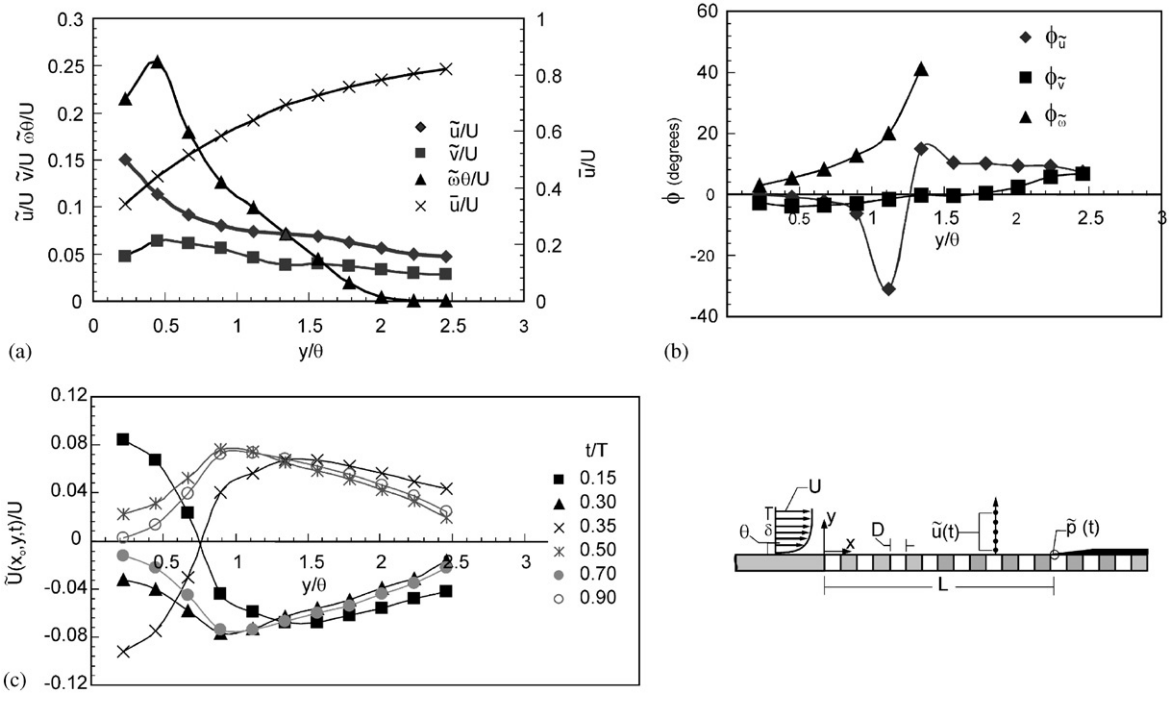

Fig. 8. Variation of amplitude and phase of organized velocity fluctuations and their corresponding phase angles across the shear layer at locations indicated in the schematic. Hole diameter is $D/\theta = 0.85$. Plot (a) shows the amplitudes of the longitudinal and transverse velocity fluctuations $\tilde{u}/U$and $\tilde{v}/U$, as well as the vorticity $\tilde{w}\theta/U$, and the time-averaged longitudinal velocity $\bar{u}/U$, in which U is the freestream velocity, as a function of transverse distance y/θ across the shear layer, in which θ is momentum thickness. Plot (b) shows the phase angle ϕ of the velocity fluctuations ϕ_u and ϕ_v, as well as vorticity fluctuations ϕ_w as a function of y/θ. Plot (c) shows the instantaneous distributions of the longitudinal velocity fluctuations $\tilde{u}(x_o, y, t)/U$as a function of distance y/θ. Data were acquired at $0.8L$. Length of perforated plate is $L/\theta = 17.2$. Dimensionless frequency of oscillation is $fL/U = 0.53$.

7. Quantitative visualization of flow structure

The organized fluctuations described in the foregoing sections are associated with time sequences of global visualization of the flow structure. Fig. 9 shows patterns of instantaneous vorticity ω and velocity correlation $\langle u'v' \rangle$ over five frames N of the cinema sequence. The organized cluster of vorticity contains small-scale concentrations of vorticity. At increasing values of N, the cluster of elongated vorticity becomes more focused and is swept above the upper surface of the impingement edge. The corresponding patterns of the instantaneous correlation $\langle u'v' \rangle$ generally retain their integrity as they are swept downstream along the surface of the plate. Again, small-scale concentrations of $\langle u'v' \rangle$ are evident.

The spanwise nature of the instantaneous flow structure was examined using the laser sheet and camera arrangements shown in Fig. 10. The laser sheet was oriented vertically, such that it was parallel to the surface of the plate, and its center-line was 1 mm from the surface.

Fig. 11 shows the instantaneous patterns of longitudinal u velocity vectors as a function of frame number N^* in a cinema sequence. Dark regions correspond to high velocity, and light regions to low velocity. For the smallest hole pattern, for which organized oscillations occur, the images at $N^* = 0$, 2 and 4, show the onset of a well-defined front, i.e., a sharply defined interface between low and high magnitudes of u vectors, the streamwise striations of large

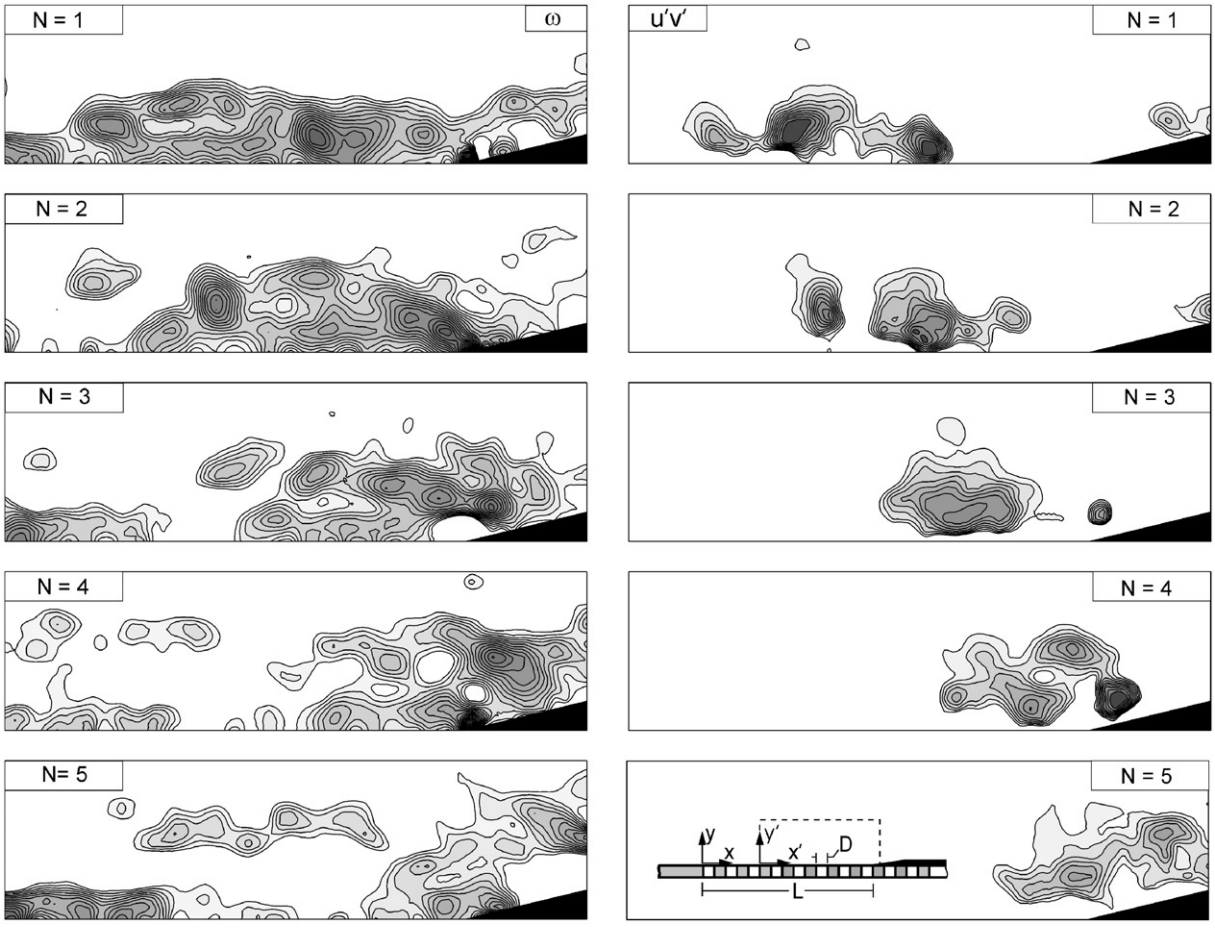

Fig. 9. Time sequence of contours of constant instantaneous vorticity and instantaneous velocity correlation. Diameter of holes in plate is $D/\theta = 0.85$. N is the frame number of the cinema sequence. One complete cycle of oscillation extends from frame $N = 1$ through frame $N = 17$. For the vorticity contours, the minimum and incremental values are $w_{\min} = -6\,s^{-1}$ and $\Delta w_{\min} = -2\,s^{-1}$. For instantaneous velocity correlation, minimum and incremental values are $[\langle u'v' \rangle / U^2]_{\min} = -3.7 \times 10^{-3}$ and $[\langle u'v' \rangle / U^2] = 3.7 \times 10^{-3}$. Upper boundary of each image corresponds to a distance of $y = 3.36\ \theta$ from surface of the perforated plate.

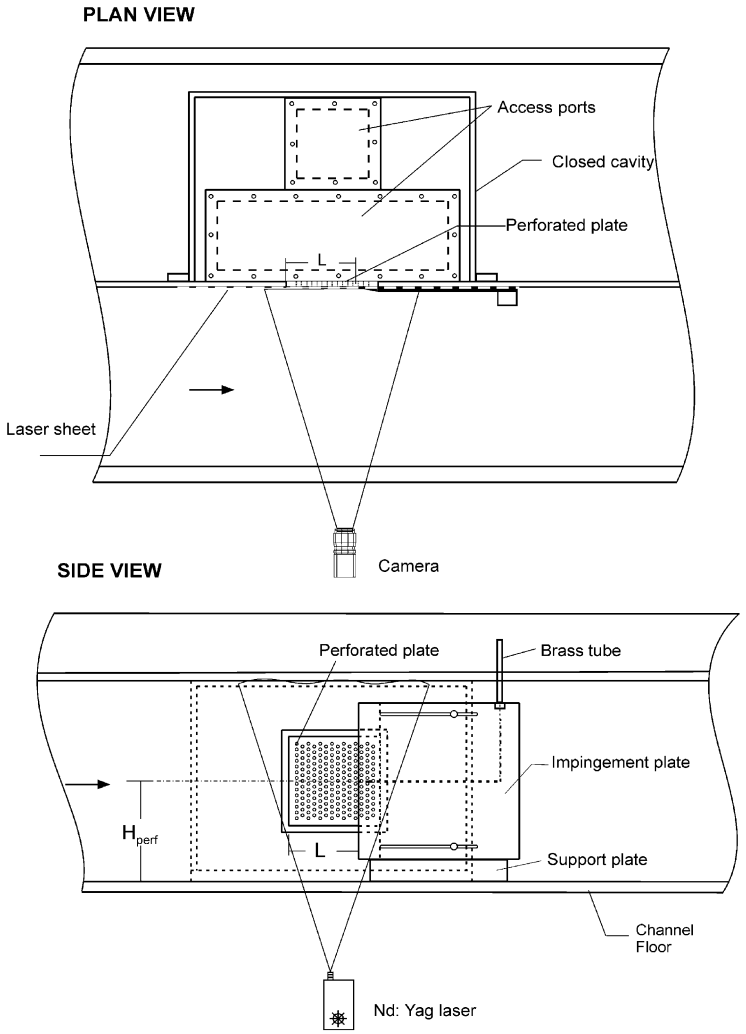

Fig. 10. Views of perforated plate test-section showing orientation and location of laser, generated laser sheet, camera and field of view for laser sheet close to surface of perforated plate.

amplitude vectors notwithstanding. The advancement of this front from left to right is in accord with the movement of the patterns of instantaneous vorticity ω and Reynolds stress correlation $\langle u'v' \rangle$ with increasing cinema frame sequence N shown in Fig. 9.

On the other hand, for the largest hole pattern, represented by the bottom set of images of Fig. 11, a well-defined front does not occur. Rather, regions of high and low velocity appear to be randomly distributed over the surface of the plate. This lack of organization is in agreement with the nature of the spectra given in Fig. 5, for which no well-defined spectral component is evident.

8. Concluding remarks

Fully turbulent inflow past a perforated plate can give rise to highly coherent, self-sustained oscillations. This type of long wavelength instability is fundamentally different from the instability typically associated with local instabilities past the individual holes or orifices in a perforated plate. It is robust and rapidly emerges above the background level of the flow, even in the absence of acoustic-resonant coupling.

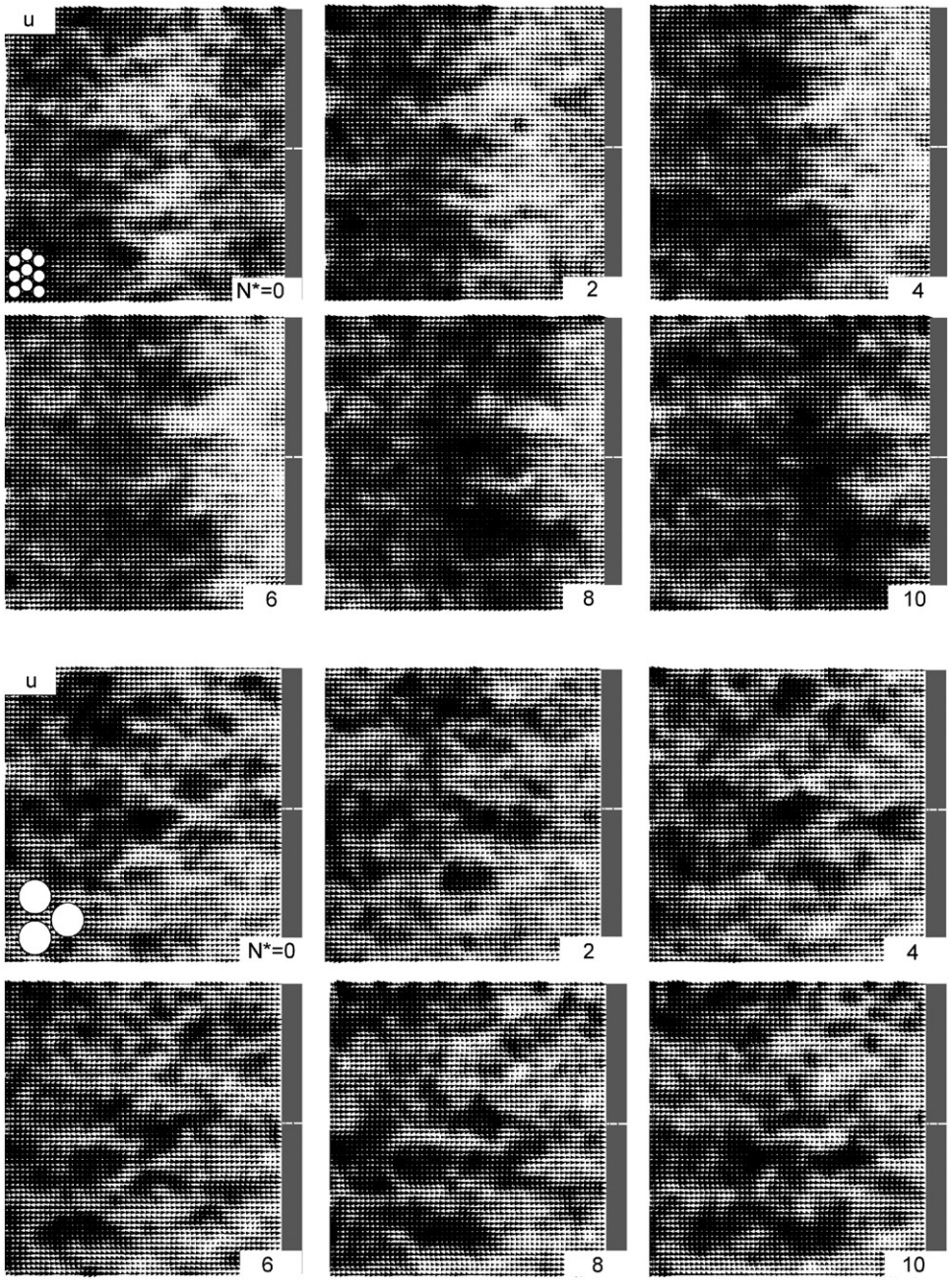

Fig. 11. Patterns of instantaneous vectors of the longitudinal (streamwise) component of velocity u for perforated plates having a small hole $D/\theta = 0.85$, corresponding to the top two rows of images and a relatively large hole $D/\theta = 3.38$, represented by the bottom two rows of images. N^* represents the frame number of the cinema sequence. For the case of the small hole $D/\theta = 0.85$, the oscillation is relatively coherent, and its period extends from $N^* = 0$ to $N^* = 16$.

In essence, the primary findings of the present study are as follows:

(1) Well-defined spectral peaks of both the pressure fluctuation at the effective trailing-end of the perforated plate, as well as in the unsteady shear layer along the plate, extend well above the background turbulence level.
(2) For an effective hole diameter D normalized by the momentum thickness θ of the turbulent boundary layer, D/θ, of the order of unity, relatively large amplitude oscillations occur, and the amplitude of the corresponding spectral

peak is sharp. As the hole diameter is increased above this value, the amplitude of the oscillation decreases and the spectral peak becomes ill-defined until, at a value of $D/\theta \sim 4$, detectable oscillations are no longer evident. Further investigations should address the effect of the thickness t of the perforated plate, and its effectiveness as a normalizing parameter, i.e., normalization of the hole diameter D by t, D/t. The relative sensitivity of the oscillation to variations in inflow momentum thickness θ and t could thereby be directly assessed. Such additional studies could also provide clues to the effect of very small values of D, while open area ratio is maintained constant, on the coherence of the self-sustained oscillation.

(3) Even when the amplitude of oscillation is significantly attenuated, but still detectable, it is demonstrated that as the effective length L of the perforated plate is varied, the dimensionless frequency fL/U remains essentially constant, for all values of hole diameter D. This observation reaffirms the view that the oscillation is indeed a long-wavelength phenomenon that is not directly influenced by the scale of the individual holes of diameter D of the plate.

(4) Patterns of time-averaged Reynolds stress show that two distinct regions occur. One region is relatively close to the perforated plate and is associated with the interaction between the shear flow and the perforations, and the other region, which is located well above the first, is associated with a classical turbulent boundary layer. For the perforated plate having holes of diameter $D/\theta \sim 1$, which give rise to the most organized and largest amplitude oscillations, the peak amplitude of Reynolds stress occurs very close to the surface of the perforated plate. Furthermore, this pattern of Reynolds stress shows an organized cell-like structure with a characteristic wavelength of the order of the hole diameter. In contrast, for the largest hole diameter $D/\theta \sim 4$, for which the organized component has an undetectable amplitude, the pattern of Reynolds stress takes on a less ordered form and its peak value is substantially smaller than for the case for which organized oscillations occur.

(5) Distributions of amplitudes of the spectral peaks of the longitudinal and transverse (organized) velocity fluctuations in the vicinity of the trailing-end of the plate show a highly organized form, with relatively large amplitudes at the effective trailing-end of the plate. These localized regions of high amplitude are associated with a source-like region, which involves an upstream influence that sustains the long wavelength oscillation.

(6) The spanwise structure of the flow pattern close to the surface of the perforated plate shows a well-organized, yet irregular, advancing front along the surface of the plate for the case where highly coherent, self-sustained oscillations occur. This observation indicates that even though the oscillations are highly coherent, the spanwise structure of the shear layer in the immediate vicinity of the plate is not highly correlated along the span, in contrast to what one typically observes for a free shear flow. On the other hand, for the case where self-sustained oscillations do not occur, no such advancing front is evident.

Acknowledgements

The authors are grateful to the Office of Naval Research (Grant No. N00014-01-1-0606) for financial support of this research program, which was monitored by Dr Pat Purtell. Dr Ted Farabee of the Naval Surface Warfare Center, Carderock, Maryland, provided insightful advice during the course of this investigation. The second author (A. Pinarbasi) acknowledges a research grant provided by the Fulbright Commission. The first author (C. Ozalp) was supported jointly by Lehigh University and Cukurova University during his research leave and as a Research Assistant by Cukurova University prior to and following his leave.

References

Adams, W.J., 1974. The design of reactive silencers for internal combustion engines. Institute of Sound and Vibration Research, Interim Report, University of Southampton.

Bauer, A.B., Chapkis, R.L., 1977. Noise generated by boundary layer interaction with perforated acoustic liners. Journal of Aircraft 14, 157–160.

Celik, E., Rockwell, D., 2003. Shear layer oscillation along a perforated surface: a self-excited large-scale instability. Physics of Fluids 14 (12), 4444–4448.

Dean, P., 1972. On the measurement of the local acoustic impedance of the walls of flow ducts and its use in predicting sound attenuation. Ph.D. Thesis, University of Southampton.

Dickey, N.S., Selamet, A., Ciray, M.S., 2001. An experimental study of the impedance of perforated plates with grazing flow. Journal of the Acoustical Society of America 110, 2360–2370.

Howe, M.S., 1996. Energy conservation and the damping of flexural waves by vorticity production. Journal of Sound and Vibration 190, 1–19.

Howe, M.S., 1997. Sound generated by turbulence and discrete vortices interacting with a perforated elastic plate in low-mach-number flow. Quarterly Journal of Mechanics & Applied Mathematics 50, 279–301.

Johansen, J.B., Smith, C.R., 1983. The Effects of Cylindrical Surface Modifications on Turbulent Boundary Layers, Report FM-3, Department of Mechanical Engineering and Mechanics. Lehigh University, Bethlehem, PA.

Lin, J.-C., Rockwell, D., 2001. Organised oscillations of an initially turbulent flow past a cavity. AIAA Journal 39, 1139–1151.

Maung, P.M., Howe, M.S., Mckinley, G.H., 1999. Experimental investigation of the damping of structural vibrations by vorticity production. Journal of Sound and Vibration 220, 297–312.

Medved, B.L., 1993. Some acoustic features of perforated test section walls with splitter plates. AIAA Journal 31, 1885–1890.

Meyer, E., Mechel, F., Kurtze, G., 1958. Experiments on the influence of flow on sound attenuation in absorbing ducts. Journal of the Acoustical Society of America 30, 165–174.

Nelson, P.A., 1982. Noise generated by flow over perforated surfaces. Journal of Sound and Vibration 83, 11–26.

Ronneberger, D., 1980. The dynamics of shearing flow over a cavity—a visual study related to the acoustic impedance of small orifices. Journal of Sound and Vibration 71, 565–581.

Tsui, C.Y., Flandro, G.A., 1977. Self-induced sound generation by flow over perforated duct liners. Journal of Sound and Vibration 50, 315–331.

Zoccola, P.J., 2002. Excitation by flow over an obstructed opening. ASME IMECE2002/NCA-33374.